ARTICLE

Enhanced 1520 nm Photoluminescence from Er^{3+} Ions in Di-erbium-carbide Metallofullerenes $(Er_2C_2)@C_{82}$ (Isomers I, II, and III)

Yasuhiro Ito,[†] Toshiya Okazaki,[‡] Shingo Okubo,[‡] Masahiro Akachi,[†] Yutaka Ohno,[§] Takashi Mizutani,[§] Tetsuya Nakamura,[∥] Ryo Kitaura,[†] Toshiki Sugai,[†] and Hisanori Shinohara[†,*]

[†]Department of Chemistry and Institute for Advanced Research, Nagoya University, Nagoya 464-8602, Japan, [‡]Research Center for Advanced Carbon Materials, National Institute of Advanced Industrial Science and Technology (AIST), Tsukuba 305-8565, Japan, [§]Department of Quantum Engineering, Nagoya University, Furo-cho, Chikusa-ku, Nagoya 464-8603, Japan, and [∥]Japan Synchrotron Radiation Research Institute, SPring-8, Sayo, Hyogo 679-5198, Japan

ABSTRACT Di-erbium and di-erbium-carbide endohedral metallofullerenes with a C_{82} cage such as $Er_2@C_{82}$ (isomers I, II, and III) and $(Er_2C_2)@C_{82}$ (isomers I, II, and III) have been synthesized and chromatographically isolated (99%). The structures of $Er_2@C_{82}$ (I, II, III) and $(Er_2C_2)@C_{82}$ (I, II, III) metallofullerenes are characterized by comparison with the UV–vis–NIR absorption spectra of $(Y_2C_2)@C_{82}$ (I, II, III), where molecular symmetries of the structures are determined to be C_s, C_{2v} and C_{3v}, respectively. Furthermore, enhanced near-infrared photoluminescence (PL) at 1520 nm from Er^{3+} ions in $Er_2@C_{82}$ (I, III) and $(Er_2C_2)@C_{82}$ (I, III) have been observed at room temperature. The PL intensities have been shown to depend on the symmetry of the C_{82} cage. In particular, the PL intensity of $(Er_2C_2)@C_{82}$ (III) has been the strongest among the isomers of $Er_2@C_{82}$ and $(Er_2C_2)@C_{82}$. Optical measurements indicate that the PL properties of $Er_2@C_{82}$ (I, II, III) and $(Er_2C_2)@C_{82}$ (I, II, III) correlate strongly with the absorbance at 1520 nm and the HOMO–LUMO energy gap of the C_{82} cage.

KEYWORDS: metallofullerene · erbium · photoluminescence · metal-carbide endohedral fullerene

*Address correspondence to noris@cc.nagoya-u.ac.jp.

Received for review September 14, 2007 and accepted November 28, 2007.

Published online December 8, 2007.
10.1021/nn700235z CCC: $37.00

During the past decade, significant interest has been focused on endohedral metallofullerenes (MFs) for their structural, magnetic, and optical novelties.[1] Since the discovery of MF encapsulated scandium trimer, Sc_3C_{82},[2–4] cluster endohedral MFs, where tri-metal-nitride clusters,[5,6] metal-carbide clusters,[7–15] and metal-hydrocarbon clusters[16] are encapsulated in the hollow space of fullerenes, have been recognized as a new type of endohedral MFs. Moreover, metal-carbide endohedral MFs have been identified as one of the cluster endohedral fullerenes encapsulating the metal-carbide clusters M_2C_2 (M = Sc, Y) and Sc_3C_2.[7–15]

One of the most interesting characteristic properties of the MFs encapsulating rare earth metal atoms, particularly lanthanide metal atoms, is the near-infrared (NIR) photoluminescence (PL) due to the f–f transition of M^{3+} (or M^{2+}) in fullerene cages. However, only erbium (Er) MFs so far have exhibited NIR PL, because fullerenes generally have absorption bands in the visible and NIR region. In the past, pioneering works on the PL measurements for $Er_2@C_{82}$ have been reported by Alford and co-workers and Dorn and co-workers.[17–19] The PL observed from $Er_2@C_{82}$ in CS_2, decalin solution and thin film at low temperature corresponds well with that expected for the $^4I_{13/2} \rightarrow {}^4I_{15/2}$ transition of the Er^{3+} ion. Furthermore, the PL can also be obtained from trierbium nitride clusters encapsulated in MFs: $(Er_3N)@C_{80}$ in CS_2 solution.[6,20]

However, the cage size and isomer separation of di-erbium MFs has not been performed completely yet judging from the results of laser-desorption time-of-flight (LD-TOF) mass and UV–vis–NIR absorption spectra in these reports.[17–19] Inoue *et al.* suggested that there are three isomers of $Er_2@C_{82}$, that is, isomers of I, II, and III, in comparison with the studies on $(Y_2C_2)@C_{82}$.[8,9] We have found that $Er_2@C_{82}$ and $(Er_2C_2)@C_{82}$ are normally very difficult to fully separate from each other even with elaborate high-performance liquid chromatography (HPLC) techniques. To obtain pure $Er_2@C_{82}$ and $(Er_2C_2)@C_{82}$, repeated recycling HPLC has been necessary. Therefore, details of PL properties of di-erbium MFs should be investigated in reference to those of di-erbium-carbide MFs, because both $Er_2@C_{82}$ and $(Er_2C_2)@C_{82}$ have exactly the same mass number.

Here, we report the synthesis and isolation of three isomers of di-erbium MFs $Er_2@C_{82}$ (I, II, III) and di-erbium-carbide MFs $(Er_2C_2)@C_{82}$ (I, II, III). The cage symmetries of $Er_2@C_{82}$ (I, II, III) and $(Er_2C_2)@C_{82}$ (I, II, III) can be determined to be $C_s(6)$, $C_{2v}(9)$, and $C_{3v}(8)$, respectively, by comparison with the UV–vis−NIR absorption spectra of $(Y_2C_2)@C_{82}$ (I, II, III) with known structures.[8,9] In particular, we have found that $(Er_2C_2)@C_{82}$ (III) has exhibited the strongest PL in isomer-separated $Er_2@C_{82}$ (I, II, III) and $(Er_2C_2)@C_{82}$ (I, II, III) in CS_2 solution. The results suggest that the presence of encapsulated C_2 molecules widens the HOMO–LUMO gap of the C_{82} cage and does not contribute to the f−f transition of the encapsulated Er^{3+}. The encapsulated C_2 molecule enhances the PL intensity by increasing the efficiency of the energy transfer from the C_{82} cage to the encapsulated Er^{3+}.

RESULTS AND DISCUSSION

UV–vis−NIR Absorption Spectra of Erbium Metallofullerene Isomers. The details of separation and isolation of erbium metallofullerene isomers are in the Supporting Information (Figure S1).

UV–vis−NIR absorption spectra of three isomers of $(Er_2C_2)@C_{82}$ in CS_2 solution, normalized with the absorbance at 400 nm, are shown in Figure 1a−c. The corresponding peak wavelengths and onsets are shown in Table 1. The absorption spectra of $(Er_2C_2)@C_{82}$ (I, II, III) are different from each other. The spectrum of $(Er_2C_2)@C_{82}$ (I) shows pronounced peaks at 634, 718, 794, 1054, and 1198 nm. The onset of the spectrum is at about 1550 nm. The spectrum of $(Er_2C_2)@C_{82}$ (II) shows pronounced peaks at 820 and 916 nm and broad absorption bands at 1474 and 1786 nm. The onset of $(Er_2C_2)@C_{82}$ (II) does not occur until 2400 nm, suggesting a small HOMO–LUMO energy gap. The solubility of $(Er_2C_2)@C_{82}$ (II) in CS_2 is much lower than that of the other two isomers. The absorption feature of $(Er_2C_2)@C_{82}$ (III) is less pronounced than the other two isomers. The characteristic absorption peaks are observed at 686 and 884 nm, and weak absorption bands are also seen at about 570, 790, and 1010 nm. The onset of the spectrum is at about 1250 nm, suggesting that the isomer has a large HOMO–LUMO energy gap compared with the other two isomers. This is consistent with the observation that isomer III is the most abundant isomer among the three $(Er_2C_2)@C_{82}$ isomers.

It is difficult to determine the molecular symmetries of the isomers of $(Er_2C_2)@C_{82}$ by ^{13}C NMR because of the presence of paramagnets of encapsulated Er^{3+}.[21–23] We therefore compare the UV–vis−NIR absorption spectra of $(Er_2C_2)@C_{82}$ with those reported for $(Y_2C_2)@C_{82}$ with known structures (see Table 1).[8,9] The absorption spectra of $(Er_2C_2)@C_{82}$ (I, II, III) are very similar to those of $(Sc_2C_2)@C_{82}$ (I, II, III),[24] respectively. Moreover, the absorption spectra of $(Y_2C_2)@C_{82}$ (I, II, III) and

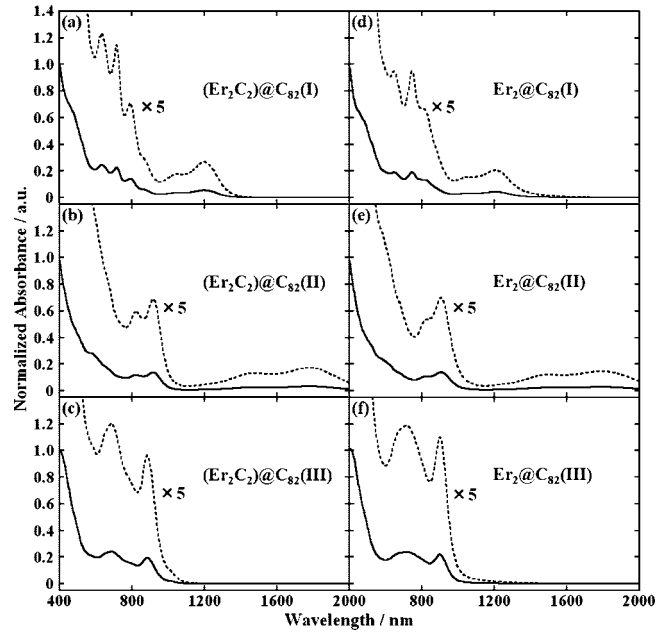

Figure 1. UV–vis−NIR absorption spectra of $(Er_2C_2)@C_{82}$ (I, II, III) and $Er_2@C_{82}$ (I, II, III) in CS_2 solvent at room temperature. These spectra are normalized with the absorbance at 400 nm, respectively.

$(Dy_2C_2)@C_{82}$ (I, II, III)[25] are almost the same as those of $(Er_2C_2)@C_{82}$ (I, II, III), respectively.

It is generally recognized that the UV–vis−NIR absorption spectra of fullerenes and MFs can reflect sensitively their cage size and symmetry.[1] For example, the spectra of $M@C_{82}$ (M = rare earth metal) show similar absorption features with a small band and onset shifts.[26] Recently, ^{13}C NMR measurements have shown that the molecular symmetries of $(Y_2C_2)@C_{82}$ (I, II, III) are C_s, C_{2v}, and C_{3v}, respectively.[8,9] Thus, the similarity of the absorption spectra between $(Y_2C_2)@C_{82}$ (I, II, III) and $(Er_2C_2)@C_{82}$ (I, II, III) suggests that the molecular symmetries of $(Er_2C_2)@C_{82}$ (I, II, III) are C_s, C_{2v}, and C_{3v}, respectively. The schematic molecular structures of $(Er_2C_2)@C_{82}$ (I, II, III) are shown in Figure 2.

UV–vis−NIR absorption spectra of $Er_2@C_{82}$ (I, II, III) in CS_2 solution, normalized with the absorbance at 400 nm, are shown in Figure 1d−f, and the corresponding peak wavelengths and onsets are shown in Table 1. The spectrum of $Er_2@C_{82}$ (I) shows pronounced peaks at 646, 746, 812, 1056 and 1208 nm. The onset of the spectrum is at about 1820 nm. The spectrum of $Er_2@C_{82}$ (II) shows pronounced peaks at 826 and 906 nm and broad absorption bands at 1500 and 1786 nm. The onset of

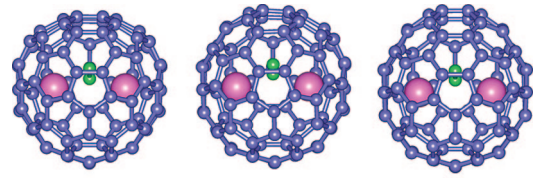

Figure 2. Schematic molecular structures of $(Er_2C_2)@C_{82}$ (I, II, III).

TABLE 1. Peak Wavelengths and Onsets Observed in UV–vis–NIR Absorption Spectra of $M_2@C_{82}$ and $(M_2C_2)@C_{82}$ (M = Er, Y)

$Er_2@C_{82}$ (nm)	$Y_2@C_{82}$ (nm)	$(Er_2C_2)@C_{82}$ (nm)	$(Y_2C_2)@C_{82}$ (nm)
		(I)	
″>646		634	629
746		718	715
812		794	791
1056		1054	1055
1208		1198	1204
1820 (onset)		1550 (onset)	1500 (onset)
		(II)	
826		820	820
906		916	910
1500		1474	1466
1786		1786	1762
2420 (onset)		2400 (onset)	2200 (onset)
		(III)	
716	714	686	684
902	909	884	880
1600 (onset)	1700 (onset)	1250 (onset)	1250 (onset)

$Er_2@C_{82}$ (II) extends to 2420 nm, suggesting a small HOMO–LUMO energy gap similar to that of $(Er_2C_2)@C_{82}$ (II). The absorption spectrum of $Er_2@C_{82}$ (III) shows only two characteristic absorption bands at 716 and 902 nm. The onset of the spectrum is at about 1600 nm.

The absorption spectra of $Er_2@C_{82}$ (I, II, III) are similar to those of $(Er_2C_2)@C_{82}$ (I, II, III), respectively, indicating that they have the same C_{82} symmetries, that is, C_s, C_{2v}, and C_{3v}. The molecular symmetries of $Er_2@C_{82}$ (I, III) are the same as those determined by single crystal structure analyses.[27,28] It is therefore reasonable that the molecular symmetries can be determined by comparing the absorption spectra of $Er_2@C_{82}$ and $(Er_2C_2)@C_{82}$.

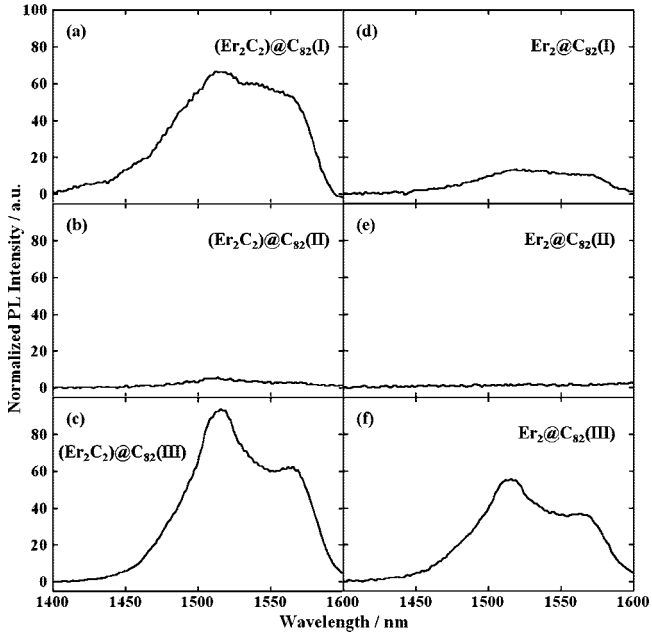

Figure 3. PL spectra of $(Er_2C_2)@C_{82}$ (I, II, III) and $Er_2@C_{82}$ (I, II, III) in CS_2 solvent at room temperature. The irradiation times are 120, 120, 1, 120, 120, and 120 s, respectively. These spectra are normalized with the absorbance at 400 nm.

Spectral Shifts Induced by Encapsulation of the C_2 Molecule. The absorption spectra of $Er_2@C_{82}$ (I, II, III) are similar to those of $(Er_2C_2)@C_{82}$ (I, II, III), respectively, suggesting that they have the same C_{82} symmetry. However, slight peak shifts are observed for the corresponding absorption bands in $Er_2@C_{82}$ and $(Er_2C_2)@C_{82}$, similar to those observed for $Y_2@C_{82}$ (III) and $(Y_2C_2)@C_{82}$ (III).[8,9] Akasaka *et al.* have reported that the absorption bands of the $La@C_{82}$ anion and cation are considerably shifted from those of neutral $La@C_{82}$.[29,30] These shifts were ascribed to the difference in the amount of negative charge on the C_{82} cage. In reference to this report, the difference in the absorption bands between $Er_2@C_{82}$ and $(Er_2C_2)@C_{82}$ can be attributed to the difference in the electron transfer from the metal atoms or metal-carbide cluster to the C_{82} cage similar to the difference between $Y_2@C_{82}$ and $(Y_2C_2)@C_{82}$.[8,9] However, the shifts of the absorption bands are much smaller than the $La@C_{82}$ case. To date, the charge density of the encapsulated C_2 molecule cannot be decided from experimental data. However, the HPLC chromatogram data indicate that the charge density of the carbon cage of $(Er_2C_2)@C_{82}$ is slightly lower than that of $Er_2@C_{82}$. This indicates that the encapsulated C_2 molecule is slightly negatively charged (not $(C_2)^{2-}$).

The onsets of the spectra of $(Er_2C_2)@C_{82}$ are also shifted compared with those of $Er_2@C_{82}$. Furthermore, the onsets at 1820, 2420, and 1600 nm of $Er_2@C_{82}$ (I, II, III) are blue-shifted to ca. 1550, 2400, and 1250 nm for $(Er_2C_2)@C_{82}$ (I, II, III), respectively. This suggests that the HOMO–LUMO gaps of $(Er_2C_2)@C_{82}$ (I, II, III) are larger than those of $Er_2@C_{82}$ (I, II, III). The encapsulation of the C_2 molecule may induce the stabilization of $(Er_2C_2)@C_{82}$, although the reason for this stabilization is not clear at present.

Enhanced 1520 nm Photoluminescence from $(Er_2C_2)@C_{82}$ (III) Metallofullerenes. Figure 3a–c shows the PL spectra of $(Er_2C_2)@C_{82}$ (I, II, III) in CS_2 solution at room temperature, which are normalized with the absorbance at 400 nm. These PL spectra correspond well with that expected for the $^4I_{13/2}(m) \rightarrow {}^4I_{15/2}(n)$ transition of the Er^{3+} ion, where (m) and (n) indicate the $J + {}^1/_2$ crystal field components of the $^4I_{13/2} \rightarrow {}^4I_{15/2}$ manifolds.[6,17–20] At room temperature, emission is observed from thermally occupied components of the upper state, and phonon scattering and absorption between the different Er levels result in strong broadening and overlap of spectral lines.

The intensities of the PL spectra differ from each other, although the structures are almost the same. The typical times required for the PL measurements of $(Er_2C_2)@C_{82}$ (I, II, III) were 120, 120, and 1 s, respectively. The PL intensity of $(Er_2C_2)@C_{82}$ (III) is about 150 times stronger than those of $(Er_2C_2)@C_{82}$ (I, II). The difference

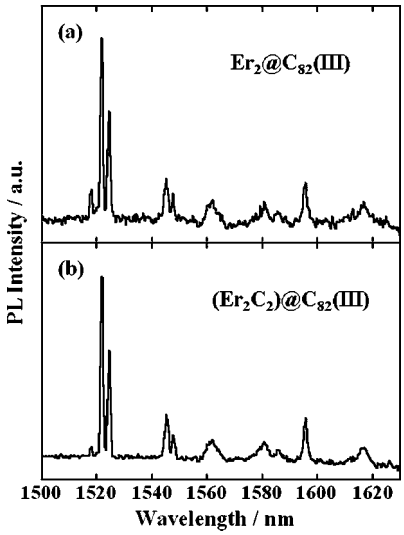

Figure 4. PL spectra of $Er_2@C_{82}$ (III) and $(Er_2C_2)@C_{82}$ (III) in bisphenol A polycarbonate thin film at 3.5 K.

is primarily caused by the existence of absorbance on these carbon cages at about 1500 nm. For example, the PL intensity of $(Er_2C_2)@C_{82}$ (II) is very weak because the carbon cage of $(Er_2C_2)@C_{82}$ (II) possesses a broad absorption band at 1500 nm, and the PL from Er^{3+} should be absorbed by the carbon cage. Similarly, the onset of the absorption spectrum of $(Er_2C_2)@C_{82}$ (I) is at about 1550 nm; $(Er_2C_2)@C_{82}$ (I) has a slight absorption at 1520 nm, which induces the reduction of the PL intensity of $(Er_2C_2)@C_{82}$ (I). $(Er_2C_2)@C_{82}$ (III), in contrast, has no absorption bands at 1520 nm, and the onset of the spectrum is at about 1250 nm, suggesting that the carbon cage of $(Er_2C_2)@C_{82}$ (III) is transparent to the PL of the encapsulated Er^{3+}.

Figure 3d−f shows PL spectra of $Er_2@C_{82}$ (I, II, III) in CS_2 solution at room temperature normalized with the absorbance at 400 nm. These spectra also correspond well with that expected for the $^4I_{13/2}(m) \rightarrow {}^4I_{15/2}(n)$ transition of the Er^{3+} ion as in $(Er_2C_2)@C_{82}$. The overall spectral structures of these spectra are almost the same. However, similar to $(Er_2C_2)@C_{82}$ isomers, the intensities of these spectra differ from each other. The difference is also due to the existence of absorbance on these carbon cages at ca. 1500 nm. $Er_2@C_{82}$ (II) does not show PL because the carbon cage of $Er_2@C_{82}$ (II) has a broad absorption band at 1500 nm similar to $(Er_2C_2)@C_{82}$ (II). $Er_2@C_{82}$ (I, III) have a slight absorption at 1520 nm; the onsets of absorption for $Er_2@C_{82}$ (I, III) are at about 1820 and 1600 nm, respectively. The absorbance of $Er_2@C_{82}$ (III) is smaller than that of $Er_2@C_{82}$ (I). Therefore, the PL intensity of $Er_2@C_{82}$ (III) is stronger than that of $Er_2@C_{82}$ (I).

Low-Temperature PL Measurements. Similar crystalline environments for Er atoms are inferred from low-temperature PL spectra between $Er_2@C_{82}$ (III) and $(Er_2C_2)@C_{82}$ (III). Figure 4 shows the PL spectra of $Er_2@C_{82}$ (III) and $(Er_2C_2)@C_{82}$ (III) in bisphenol A polycarbonate thin film at 3.5 K. The spectra consist of about eight principal lines as expected for emission from the lowest excited $^4I_{13/2}(1)$ level to the eight doubly degenerate levels of the $^4I_{15/2}$ ground manifold, which confirms a trivalent nature of the Er ions.[18] These spectra are different from those of $(Er_3N)@C_{80}$ already reported.[6] One of the notable differences is the doublet structures observed around 1520 nm in the $^4I_{13/2}(1)$ to $^4I_{15/2}(1)$ origin line. The doublet structures also observed for $(Er_2ScN)@C_{80}$ and $(ErSc_2N)@C_{80}$ are interpreted as due to two probable positions of encapsulated Er atom(s) in the C_{80} cage since such a doublet structure does not appear for $(Er_3N)@C_{80}$, suggesting that the doublet structures occur due to the symmetrical difference. Similarly, the molecular symmetries of $Er_2@C_{82}$ (III) and $(Er_2C_2)@C_{82}$ (III) are lower than those of $(Er_3N)@C_{80}$, in which both $Er_2@C_{82}$ (III) and $(Er_2C_2)@C_{82}$ (III) have C_{3v} symmetry compared with the I_h symmetry of $(Er_3N)@C_{80}$. Each encapsulated Er^{3+} in $Er_2@C_{82}$ (III) and $(Er_2C_2)@C_{82}$ (III) is, therefore, not in a geometrically equivalent position in the C_{82} cage.

The low-temperature PL spectra of $Er_2@C_{82}$ (III) and $(Er_2C_2)@C_{82}$ (III) are almost same as each other, indicating that the encapsulated C_2 molecule does not significantly vary the positions of encapsulated Er^{3+} and does not substantially restrict the internal motion of Er^{3+}. This is consistent with the reported molecular structures of $Y_2@C_{82}$ (III) and $(Y_2C_2)@C_{82}$ (III). Synchrotron X-ray diffraction with the MEM/Rietveld analysis revealed the presence of a pentagonal−dodecahedral shape of the charge density due to Y_2 in both $Y_2@C_{82}$ (III) and $(Y_2C_2)@C_{82}$ (III); the Y−Y distance is almost the same in $Y_2@C_{82}$ (III) (3.84(3) Å) and $(Y_2C_2)@C_{82}$ (III) (4.07(3) Å).[10]

These results strongly suggest that the encapsulated C_2 molecule does not affect the encapsulated

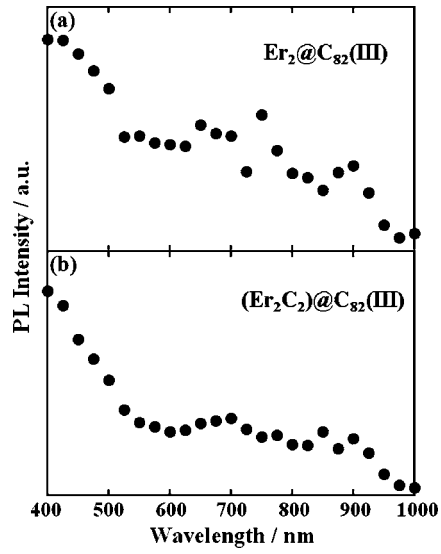

Figure 5. Excitation energy dependence on the PL intensities of $Er_2@C_{82}$ (III) and $(Er_2C_2)@C_{82}$ (III) in CS_2 solvent at room temperature.

Er^{3+}: the C_2 molecule does not affect the f−f electronic transition of the encapsulated Er^{3+}. This idea is also suggested by the X-ray absorption spectra and the PL lifetime at 1520 nm of $Er_2@C_{82}$ and $(Er_2C_2)@C_{82}$ (Supporting Information, Figures S2 and S3). However, the insertion of the C_2 molecule into the C_{82} cage does induce widening of teh HOMO–LUMO gap of the C_{82} cage. This should affect the energy transfer from the C_{82} cage to encapsulated Er^{3+}.

PL Mechanism of $Er_2@C_{82}$ and $(Er_2C_2)@C_{82}$. Figure 5 shows the excitation energy dependence on the PL intensities of $Er_2@C_{82}$ (III) and $(Er_2C_2)@C_{82}$ (III). These excitation spectra are very similar to the UV–vis−NIR absorption spectra of $Er_2@C_{82}$ (III) (cf. Figure 1f) and $(Er_2C_2)@C_{82}$ (III) (Figure 1c) between 400 and 1000 nm. If the direct absorption by Er^{3+} 4f levels is responsible for the observed emission, the corresponding atomic absorption peaks are expected to appear in the excitation spectra. However, no such distinct peaks are observed in Figure 5a,b, indicating that the absorption is primarily achieved by the C_{82} fullerene cage and that an efficient energy transfer occurs from the LUMO of the C_{82} cage to $^4I_{13/2}$ level of encapsulated Er^{3+}.

$Er_2@C_{82}$ and $(Er_2C_2)@C_{82}$ are first excited from the singlet S_0 ground state (HOMO) to the singlet S_n excited state (the exact position is not known, but higher lying than 1.24 eV) followed by a fast relaxation to the singlet S_1 (LUMO) state and then to the triplet T state (this state could not be observed by the transient absorption measurements). From this triplet state, an effective energy transfer to the $^4I_{13/2}$ first excited-state in Er^{3+} should be occurring. Finally, the $^4I_{13/2}$ would decay to the $^4I_{15/2}$ ground manifold by emitting a 1520 nm photon. The corresponding schematic energy diagram is presented in Figure 6.

The proposed energy diagram suggests that the HOMO–LUMO energy gap of the C_{82} cage influences substantially the energy transfer from the C_{82} cage to $^4I_{13/2}$ level in encapsulated Er^{3+}. As can be seen in the UV–vis−NIR absorption spectra (see Figure 1), the HOMO–LUMO energy gaps (inferred from the absorption onsets in Figure 1) of $Er_2@C_{82}$ (I, II, III) and $(Er_2C_2)@C_{82}$ (I, II, III) are 0.68, 0.51, 0.78, 0.8, 0.52, and 0.99 eV, respectively (see Table 1).

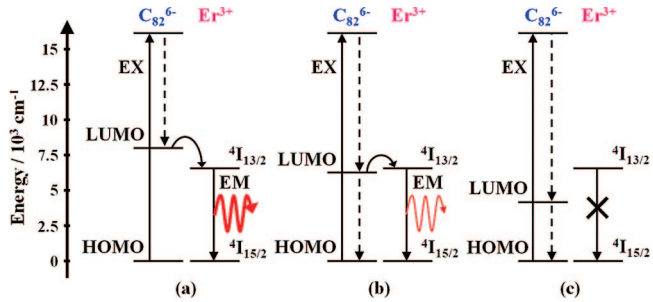

Figure 6. Schematic diagram of the energy dynamics possibly occurring in $Er_2@C_{82}$ (III) and $(Er_2C_2)@C_{82}$ (III).

By comparison of the HOMO–LUMO energy gaps of $Er_2@C_{82}$ and $(Er_2C_2)@C_{82}$ to the ground−excited ($^4I_{15/2}$−$^4I_{13/2}$) electronic state gaps of Er^{3+}, the energy diagram may be divided into three types, which are schematically shown in Figure 6a−c. Figure 6a shows the case in which the LUMO level of the C_{82} cage is higher than the $^4I_{13/2}(1)$ level of Er^{3+}. This may correspond to the $(Er_2C_2)@C_{82}$ (III) case. The energy transfer from the LUMO of the C_{82} cage to the $^4I_{13/2}$ level in encapsulated Er^{3+} should be most efficient in all the isomers of $Er_2@C_{82}$ and $(Er_2C_2)@C_{82}$. The PL intensity of $(Er_2C_2)@C_{82}$ (III) should, therefore, be the strongest. Figure 6b shows the case in which the LUMO level of the C_{82} cage and the $^4I_{13/2}(1)$ level of Er^{3+} are nearly the same. This may correspond to the cases of $Er_2@C_{82}$ (I, III) and $(Er_2C_2)@C_{82}$ (I). In this case, the energy transfer from the C_{82} cage to Er^{3+} and the relaxation to the HOMO of C_{82} might compete with each other, resulting in the reduction of the PL intensity compared with that of $(Er_2C_2)@C_{82}$ (III). The efficiency of energy transfer in $Er_2@C_{82}$ (I, III) and $(Er_2C_2)@C_{82}$ (I) can be almost the same because the PL intensities of these substances obey the Beer–Lambert law.

Figure 6c, in contrast, shows the case that LUMO level of the C_{82} cage is lower than the $^4I_{13/2}(1)$ level of Er^{3+}, which undoubtedly corresponds to $Er_2@C_{82}$ (II) and $(Er_2C_2)@C_{82}$ (II). In this case, an excited HOMO state of the C_{82} cage will rapidly decay nonradiatively to the LUMO state without transferring the energy to Er^{3+}. Thus, PL from Er^{3+} has not been observed. A similar relaxation is happening in the case of $Er@C_{82}$.[19] It is known that $Er@C_{82}$ is also nonfluorescent because the HOMO–LUMO energy gap of $Er@C_{82}$ is smaller than 0.50 eV and in addition $Er@C_{82}$ has a broad absorption band at 1500 nm similar to $Er_2@C_{82}$ (II) and $(Er_2C_2)@C_{82}$ (II). The HOMO–LUMO energy gap of the C_{82} cage, in reference to that of the ground−excited ($^4I_{15/2}$−$^4I_{13/2}$) electronic transition of Er^{3+}, is one of the most significant factors for exhibiting enhanced PL from the di-erbium MFs.

Although the encapsulated C_2 molecule does not significantly influence the f−f transition of encapsulated Er^{3+}, it widens the HOMO–LUMO energy gap of the C_{82} cage and decreases the absorbance at ca. 1520 nm. The observed PL intensity of $(Er_2C_2)@C_{82}$ was much stronger than that of $Er_2@C_{82}$. Therefore, the C_2 molecule is certainly responsible for the enhanced PL properties of the di-erbium MFs.

SUMMARY

Di-erbium MFs $(Er_2C_2)@C_{82}$ (I, II, III) and $Er_2@C_{82}$ (I, II, III) have been synthesized, isolated, and characterized by UV–vis−NIR absorption and PL spectroscopy. A comparison of the UV–vis−NIR absorption spectra with those of $(Y_2C_2)@C_{82}$ (I, II, III) indicates that each of

$(Er_2C_2)@C_{82}$ (I, II, III) and $Er_2@C_{82}$ (I, II, III) isomers has $C_s(6)$, $C_{2v}(9)$ and $C_{3v}(8)$ symmetry, respectively.

One of the most important observations here is that a di-erbium-carbide MF $(E_2C_2)@C_{82}$ (III) exhibits an intense PL from the encapsulated Er^{3+} at 1520 nm compared with other di-erbium MFs $Er_2@C_{82}$ (I, II, III). The results can be interpreted in terms of widening of the HOMO–LUMO energy gap of the C_{82} cage when C_2 is inserted between the two Er^{3+}, which results in the reduction of absorbance at ca. 1500 nm of the C_{82} cage. The PL intensity of $(E_2C_2)@C_{82}$ (III) is thus enhanced significantly compared with the other Er MFs.

EXPERIMENTAL SECTION

Er MFs were produced by the DC arc-discharge method.[1,9,31] The soot containing Er MFs was collected anaerobically and extracted by using *o*-xylene. The Er MFs $Er_2@C_{82}$ (I, II, III) and $(Er_2C_2)@C_{82}$ (I, II, III) were separated and isolated from various empty fullerenes and other Er MFs by the multistage high performance liquid chromatography (HPLC) method[9,31] with four different types of columns [5PYE (20 mm diameter × 250 mm, Nacalai Tesque, 21 mL/min flow rate), Buckyprep (20 mm diameter × 250 mm, Nacalai Tesque, 21 mL/min flow rate), Buckyclutcher-I (21.1 mm diameter × 500 mm, Regis Chemical, 10 mL/min flow rate), Buckyprep-M (20 mm diameter × 250 mm, Nacalai Tesque, 10 mL/min flow rate)] with toluene as the eluent. Details of the separation of endohedral MFs can be found elsewhere.[1]

The purity of the various isomers of $Er_2@C_{82}$ and $(Er_2C_2)@C_{82}$ was confirmed by both positive and negative laser desorption time-of-flight (LD-TOF) mass spectrometry as well as HPLC analyses. LD-TOF mass spectral data were obtained on a Shimadzu MALDI-IV mass spectrometer. UV–vis−NIR absorption spectra of $Er_2@C_{82}$ and $(Er_2C_2)@C_{82}$ were measured in CS_2 solution using a JASCO V-570 spectrophotometer. PL measurements in CS_2 solution at room temperature were performed on a Shimadzu NIR-PL system (CNF-RF) equipped with a liquid N_2 cooled InGaAs detector array. Di-erbium MFs were excited at 400 nm using a Xe lamp. The slit widths used were 20 nm for both excitation and emission. The typical scan step was 2 nm.

X-ray absorption spectra were measured at the twin helical undulators soft X-ray beamline BL25SU in SPring-8. Absorption intensities were recorded by the total electron yield method (TEY) applying a bias voltage of 36 V to the thin films of di-erbium MFs and the powder of Er_2O_3.

PL lifetimes of the various erbium fullerenes in CS_2 solution were measuremed by using an optical parametric amplifier (Spectra Physics OPA-800) with 6 μJ, 1 ps pulse of exciting light at 515 nm, and a liquid N_2 cooled InGaAs photomultiplier (HAMAMATSU R5509-73) with a time resolution of 40 ns. PL detection was performed on the $^4I_{13/2}(1)-{}^4I_{15/2}(1)$ transition at 1520 nm.

Excitation spectra in CS_2 solution were obtained by using a HORIBA SPEX Fluorolog 3-2 TRIAX spectrofluorometer equipped with a near-infrared photomultiplier module (HAMAMATSU H9170-75). The slit width and scan steps were 10 and 25 nm, respectively, for both excitation and emission. The observation was made at the $^4I_{13/2}(1)-{}^4I_{15/2}(1)$ transition at 1520 nm. Low-temperature PL measurements were carried out using a HORIBA SPEX Fluorolog 3-2 TRIAX spectrofluorometer and a Ti/sapphire laser (Spectra Physics 3900S) for excitation. The samples were excited at 700 nm and the slit width was 1.0 nm for excitation. Di-erbium MFs were mixed with bisphenol A polycarbonate using *o*-dichlorobenzene and coated on the quartz glass.[32]

Acknowledgment. We thank Professor T. Kato (Josai University) for conducting low-temperature PL measurements. This work was supported by the JST CREST Program for Novel Carbon Nanotube Materials and the 21st Century COE programs of JSPS.

Supporting Information Available: Details of separation and isolation of erbium metallofullerene isomers, charge states of encapsulated Er^{3+} in $Er_2@C_{82}$ (III) and $(Er_2C_2)@C_{82}$ (III), and 1520 nm photoluminescence lifetimes of $Er_2@C_{82}$ (III) and $(Er_2C_2)@C_{82}$ (III). This material is available free of charge *via* the Internet at http://pubs.acs.org.

REFERENCES AND NOTES

1 Shinohara, H. Endohedral Metallofullerenes. *Rep. Prog. Phys.* **2000**, *63*, 843–892.
2 Shinohara, H.; Sato, H.; Ohkohchi, M.; Ando, Y.; Kodama, T.; Shida, T.; Kato, T.; Saito, Y. Encapsulation of a Scandium Trimer in C_{82}. *Nature* **1992**, *357*, 52–54.
3 Kato, T.; Bandou, S.; Inakuma, M.; Shinohara, H. ESR Study on Structures and Dynamics of $Sc_3@C_{82}$. *J. Phys. Chem.* **1995**, *99*, 856–858.
4 Takata, M.; Nishibori, E.; Sakata, M.; Inakuma, M.; Yamamoto, E.; Shinohara, H. Triangle Scandium Cluster Imprisoned in a Fullerene Cage. *Phys. Rev. Lett.* **1999**, *83*, 2214–2217.
5 Stevenson, S.; Rice, G.; Glass, T.; Harich, K.; Cromer, F.; Jordan, M. R.; Craft, J.; Hadju, E.; Bible, R.; Olmstead, M. M.; Maitra, K.; Fisher, A. J.; Balch, A. L.; Dorn, H. C. Small-Bandgap Endohedral Metallofullerenes in High Yield and Purity. *Nature* **1999**, *401*, 55–57.
6 Macfarlane, R. M.; Bethune, D. S.; Stevenson, S.; Dorn, H. C. Fluorescence Spectroscopy and Emission Lifetimes of Er^{3+} in $Er_xSc_{3-x}N@C_{80}$ ($x = 1$–3). *Chem. Phys. Lett.* **2001**, *343*, 229–234.
7 Wang, C. R.; Kai, T.; Tomiyama, T.; Yoshida, T.; Kobayashi, Y.; Nishibori, E.; Takata, M.; Sakata, M.; Shinohara, H. A Scandium Carbide Endohedral Metallofullerene: $(Sc_2C_2)@C_{84}$. *Angew. Chem., Int. Ed.* **2001**, *40*, 397–399.
8 Inoue, T.; Tomiyama, T.; Sugai, T.; Shinohara, H. Spectroscopic and Structural Study of Y_2C_2 Carbide Encapsulating Endohedral Metallofullerene: $(Y_2C_2)@C_{82}$. *Chem. Phys. Lett.* **2003**, *382*, 226–231.
9 Inoue, T.; Tomiyama, T.; Sugai, T.; Okazaki, T.; Suematsu, T.; Fujii, N.; Utsumi, H.; Nojima, K.; Shinohara, H. Trapping a C_2 Radical in Endohedral Metallofullerenes: Synthesis and Structures of $(Y_2C_2)@C_{82}$ (Isomers I, II, and III). *J. Phys. Chem. B* **2004**, *108*, 7573–7579.
10 Nishibori, E.; Narioka, S.; Takata, M.; Sakata, M.; Inoue, T.; Shinohara, H. A C_2 Molecule Entrapped in the Pentagonal-Dodecahedral Y_2 Cage in $Y_2C_2@C_{82}$(III). *ChemPhysChem* **2006**, *7*, 345–348.
11 Nishibori, E.; Ishihara, M.; Takata, M.; Sakata, M.; Ito, Y.; Inoue, T.; Shinohara, H. Bent (Metal)(2)C_2 Clusters Encapsulated in $(Sc_2C_2)@C_{82}$(III) and $(Y_2C_2)@C_{82}$(III) Metallofullerenes. *Chem. Phys. Lett.* **2006**, *433*, 120–124.
12 Nishibori, E.; Terauchi, I.; Sakata, M.; Takata, M.; Ito, Y.; Sugai, T.; Shinohara, H. High-Resolution Analysis of $(Sc_3C_2)@C_{80}$ Metallofullerene by Third Generation Synchrotron Radiation X-ray Powder Diffraction. *J. Phys. Chem. B* **2006**, *110*, 19215–19219.
13 Iiduka, Y.; Wakahara, T.; Nakahodo, T.; Tsuchiya, T.; Sakuraba, A.; Maeda, Y.; Akasaka, T.; Yoza, K.; Horn, E.; Kato, T.; Liu, M. T. H.; Mizorogi, N.; Kobayashi, K.; Nagase, S. Structural Determination of Metallofullerene Sc_3C_{82} Revisited: A Surprising Finding. *J. Am. Chem. Soc.* **2005**, *127*, 12500–12501.
14 Iiduka, Y.; Wakahara, T.; Nakajima, K.; Tsuchiya, T.; Nakahodo, T.; Maeda, Y.; Akasaka, T.; Mizorogi, N.;

Nagase, S. ^{13}C NMR Spectroscopic Study of Scandium Dimetallofullerene, $Sc_2@C_{84}$ vs. $(Sc_2C_2)@C_{82}$. *Chem. Commun.* **2006**, 2057–2059.
15 Shi, Z. Q.; Wu, X.; Wang, C. R.; Lu, X.; Shinohara, H. Isolation and Characterization of $Sc_2C_2@C_{68}$: A Metal-Carbide Endofullerene with a Non-IPR Carbon Cage. *Angew. Chem., Int. Ed.* **2006**, *45*, 2107–2111.
16 Krause, M.; Ziegs, F.; Popov, A. A.; Dunsch, L. Entrapped Bonded Hydrogen in a Fullerene: The Five-Atom Cluster Sc_3CH in C_{80}. *ChemPhysChem* **2007**, *8*, 537–540.
17 Ding, X. Y.; Alford, J. M.; Wright, J. C. Lanthanide Fluorescence from Er^{3+} in $Er_2@C_{82}$. *Chem. Phys. Lett.* **1997**, *269*, 72–78.
18 Macfarlane, R. M.; Wittmann, G.; vanLoosdrecht, P. H. M.; deVries, M.; Bethune, D. S.; Stevenson, S.; Dorn, H. C. Measurement of Pair Interactions and 1.5 μm Emission from Er^{3+} Ions in a C_{82} Fullerene Cage. *Phys. Rev. Lett.* **1997**, *79*, 1397–1400.
19 Hoffman, K. R.; Norris, B. J.; Merle, R. B.; Alford, M. Near infrared Er^{3+} Photoluminescence from Erbium Metallofullerenes. *Chem. Phys. Lett.* **1998**, *284*, 171–176.
20 Jones, M. A. G.; Taylor, R. A.; Ardavan, A.; Porfyrakis, K.; Briggs, G. A. D. Direct Optical Excitation of a Fullerene-Incarcerated Metal Ion. *Chem. Phys. Lett.* **2006**, *428*, 303–306.
21 Kodama, T.; Ozawa, N.; Miyake, Y.; Sakaguchi, K.; Nishikawa, H.; Ikemoto, I.; Kikuchi, K.; Achiba, Y. Structural Study of Three Isomers of $Tm@C_{82}$ by ^{13}C NMR Spectroscopy. *J. Am. Chem. Soc.* **2002**, *124*, 1452–1455.
22 Wakahara, T.; Kobayashi, J.; Yamada, M.; Maeda, Y.; Tsuchiya, T.; Okamura, M.; Akasaka, T.; Waelchli, M.; Kobayashi, K.; Nagase, S.; Kato, T.; Kako, M.; Yamamoto, K.; Kadish, K. M. Characterization of $Ce@C_{82}$ and its Anion. *J. Am. Chem. Soc.* **2004**, *126*, 4883–4887.
23 Yamada, M.; Wakahara, T.; Lian, Y. F.; Tsuchiya, T.; Akasaka, T.; Waelchli, M.; Mizorogi, N.; Nagase, S.; Kadish, K. M. Analysis of Lanthanide-Induced NMR Shifts of the $Ce@C_{82}$ Anion. *J. Am. Chem. Soc.* **2006**, *128*, 1400–1401.
24 Inakuma, M.; Yamamoto, E.; Kai, T.; Wang, C. R.; Tomiyama, T.; Shinohara, H.; Dennis, T. J. S.; Hulman, M.; Krause, M.; Kuzmany, H. Structural and Electronic Properties of Isomers of $Sc_2@C_{84}$(I, II, III): ^{13}C NMR and IR/Raman Spectroscopic Studies. *J. Phys. Chem. B* **2000**, *104*, 5072–5077.
25 Tagmatarchis, N.; Shinohara, H. Production, Separation, Isolation, and Spectroscopic Study of Dysprosium Endohedral Metallofullerenes. *Chem. Mater.* **2000**, *12*, 3222–3226.
26 Akiyama, K.; Sueki, K.; Kodama, T.; Kikuchi, K.; Ikemoto, I.; Katada, M.; Nakahara, H. Absorption Spectra of Metallofullerenes $M@C_{82}$ of Lanthanoids. *J. Phys. Chem. A* **2000**, *104*, 7224–7226.
27 Olmstead, M. M.; de Bettencourt-Dias, A.; Stevenson, S.; Dorn, H. C.; Balch, A. L. Crystallographic Characterization of the Structure of the Endohedral Fullerene $Er_2@C_{82}$ Isomer I with C_s Cage Symmetry and Multiple Sites for Erbium along a Band of Ten Contiguous Hexagons. *J. Am. Chem. Soc.* **2002**, *124*, 4172–4173.
28 Olmstead, M. M.; Lee, H. M.; Stevenson, S.; Dorn, H. C.; Balch, A. L. Crystallographic Characterization of Isomer 2 of $Er_2@C_{82}$ and Comparison with Isomer 1 of $Er_2@C_{82}$. *Chem. Commun.* **2002**, 2688–2689.
29 Akasaka, T.; Wakahara, T.; Nagase, S.; Kobayashi, K.; Waelchli, M.; Yamamoto, K.; Kondo, M.; Shirakura, S.; Maeda, Y.; Kato, T.; Kako, M.; Nakadaira, Y.; Gao, X.; Van Caemelbecke, E.; Kadish, K. M. Structural Determination of the $La@C_{82}$ Isomer. *J. Phys. Chem. B* **2001**, *105*, 2971–2974.
30 Akasaka, T.; Wakahara, T.; Nagase, S.; Kobayashi, K.; Waelchli, M.; Yamamoto, K.; Kondo, M.; Shirakura, S.; Okubo, S.; Maeda, Y.; Kato, T.; Kako, M.; Nakadaira, Y.; Nagahata, R.; Gao, X.; Van Caemelbecke, E.; Kadish, K. M. $La@C_{82}$ Anion. An Unusually Stable Metallofullerene. *J. Am. Chem. Soc.* **2000**, *122*, 9316–9317.
31 Tagmatarchis, N.; Aslanis, E.; Prassides, K.; Shinohara, H. Mono-, Di- and Trierbium Endohedral Metallofullerenes: Production, Separation, Isolation, and Spectroscopic Study. *Chem. Mater.* **2001**, *13*, 2374–2379.
32 Koltover, V. K.; Parnyuk, T. A.; Bubnov, V. P.; Laukhina, E. E.; Estrin, Y. I.; Yagubskii, E. B. Stability and Mobility of the Endohedral Metallofullerene of $La@C_{82}$ in Polycarbonate Polymer Films. *Phys. Solid State* **2002**, *44*, 529–530.